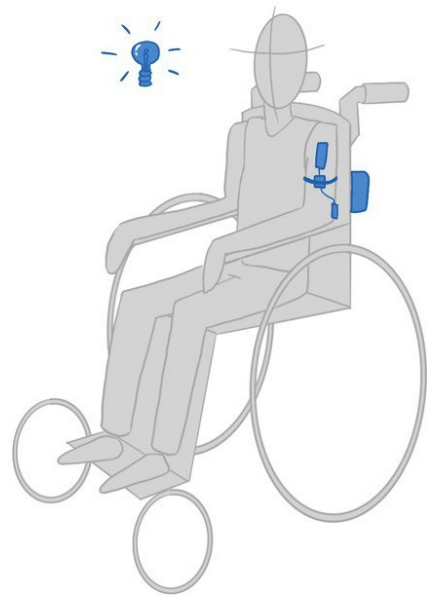


EPFL, 30TH DECEMBER 2023

SPASM AND VOLUNTARY MOVEMENT DETECTION

BIO-433 NEURAL INTERFACE

FINAL REPORT



1 Summary

1.1 Summary

The purpose of our device is to aid in the neurorehabilitation of patients with motor disorders, such as spastic quadriplegia, who face challenges in motor control due to the inability to distinguish between voluntary movements and spasms. We aim to improve an existing device into a daily usable one that is adaptable to various patients.

We suggest a wireless active flexible microneedle-array-electrode system for long-term recording of muscle activity signals (EMG) that improves the recording and filtering part. For that we first established the requirements for our new device and we came up with an innovative solutions that combine elements of existing literature, including biomedical studies on ECG recordings. Then, both the electrode and the electronics were designed, resulting in a comprehensive device. Particular attention was given to the connectors to ensure feasibility, as well as materials and dimensions.

The result is a pair of recording and reference electrode embedding arrays of 36 microneedles that are grown thanks to the MRLD method on a Parylene flexible substrate, connected via a conductive layer of Ti/Au to FFC cables to enable their pooling and transmission to the electronics. To ensure good conductivity and low impedance, a Ti/Au/PEDOT:PSS coating is applied to the microneedles. Traditional methods such as photo-lithography, etching and sputtering are used to grow the substrate and the conductive layers to ensure their feasibility in any clean-room.

The signals are filtered by a 20-1000Hz bandpass filter, amplified through the tunable gain (10,100, 1000) of an OTA amplifier. The resulting signals are converted to digital data and transmitted wirelessly thanks to a microcontroller and a bluetooth module to a computer for further processing. This involves the application of an amplitude threshold algorithm of the EMG signals enabling to distinguish between spasms and voluntary movements. The result is a feedback in form of a visual interactive application on a screen.

Theoretical characterisations of the electrodes is computed to ensure bending and stress resistance, enabling a stable and conformable interface with the curved skin. Microneedle impedance is calculated theoretically and is slightly higher than the values found in the literature. Empirical characterisations would be needed prior any real-life application to ensure biosafety of the device. A feasibility assessment is therefore conducted. Finally, a set of limitations and areas for improvement is outlined for the real device to come to life.

2 State of the Art Review

2.1 Background

In many neurological conditions, patients lack the ability to differentiate between voluntary and involuntary movements. These patients often go through physiotherapy to learn to distinguish them in order to develop voluntary motor control and to eventually be able to move their bodies. Our device has the objective to aid these neurorehabilitation processes. We focused on the specific case of cerebral palsy (CP), caused by permanent brain lesions occurring in the developing brain, and characterised by a loss in the ability to control movement and maintain posture and balance. 20% of children with CP suffer from its most drastic form, spastic quadriplegia [34]. Spastic quadriplegia is marked by significant disruptions in psycho-motor development and severe functional limitations. Developing basic mobility such as sitting, independent ambulation, or even head control is a challenge.

In 2022 Hackathealth' hackaton edition, Laura, a 5-year-old girl suffering from this neurological disorder has had a device created for her needs that was later refined thanks to founding ¹.

¹Currently, the team lacks people experienced in the domain of electronics and signal processing and would highly benefit from a course such as this one. Laura's therapist not only showed enthusiasm for our interest in redesigning the device but also agreed to disclose Laura's condition and the current device details in the context of this project.

Her therapists say that despite somaesthetic impairment due to brain lesions, children can still feel and control their movement to a certain degree. By active participation, these skills could be improved and enable the children to gain control on their bodies relying on neuronal plasticity. This assumption was proven to be right as improvements in Laura's condition were seen throughout the use of the further detailed device.

2.2 Current product

The physiotherapy session currently employs a system that comprises monitoring, signal processing, and feedback components integrated into a single device.

Muscle activity is monitored through the use of *Kendall EMG foam solid gel electrodes* [24]. These electrodes are passive Ag/AgCl electrodes that require an electrolytic gel. The placement of these electrodes depends on several criterias, including the size of the target muscle (the larger muscles the clearer and stronger the signals). The proximity of the device to the skin is crucial as it records less noise and requires less filtering. Observation of the patient's movements enables therapists to identify active muscles that require monitoring. Therefore, the child's movements are recorded not only through the device but also via a webcam and OBS studio software.

The signals are transmitted to a computer via cables. *The Cyton Box* [13] software recovers data and sends it over to the *LabStreamingLayer (LSL)* network for recording and synchronization. A Python code enables the pooling of information from the video and electrodes based on the time of each image taken. This association allows for further analysis, such as a more precise targeting of muscles. Filtering and comparing amplitudes by setting thresholds at the beginning of the session ultimately enables the distinction between voluntary movements and spasms.

Feedback is provided through an interactive application that allows the child to visualize an animation for each muscle contraction they perform. The application receives real-time data from the *Open BCI* software, analyzes it, and triggers animations. For example, when the right arm is contracted, a small cat appears on the right side of the screen, and when the left arm is contracted, the cat appears on the left. In the case of spasms, calming music is played. The levels that trigger each animation or sound can be adjusted through the graphical interface. Each motor event is specified as either a voluntary or involuntary contraction. This information is sent on the LSL network to allow for initial data analysis.

This design is advanced, but presents a few limitations such as a high noise levels and difficult daily usage. After numerous exchanges with the therapist, a list of requirements to fulfil was drawn and is summarised in 1 for our redesign of the current system.

Requirement	Reasoning	Achieved
Noise reduction	The current device has an extremely low signal to noise ratio, making the signal analysis challenging	Yes
Comfort	As we are dealing with the paediatric population, special care has to be taken to the comfort and skin reaction	Yes
Long-term monitoring	Enable its daily usage	Yes
Fewer wires	Enable children with a high range of spasm to use it without additional accelerometer	Yes
Feasibility	Would like to create it	Yes
Low-cost	Enable its production at large scale and its usage	No
Mass production	Enable to be used on a daily basis and by numerous children	No

Table 1: Requirements

2.3 Type of electrodes

The human skin is composed of three layers [31]: the stratum corneum layer (SCL), the epidermis layer (EL), and the dermis layer (DL). The SCL, consisting of dead cells and sweat/grease, presents high electrical impedance due to the lack of ion channels. When in direct contact with an electrode, the combination of the SCL and sweat/grease forms a metal-electrolyte interface, leading to the development of a half-cell potential. Factors such as capacitance of the electrode-sweat interface and resistance of sweat contribute to a polarisation effect.

To overcome the high impedance of SCL, standard Ag/AgCl electrodes require skin preparation, such as hair removal and cleaning of the skin to reduce sweat. Most importantly, they require a conductive gel. Although the gel enables good impedance, it has the disadvantage of drying out over time, resulting in measurement errors by increasing resistance and leading to motion artifacts. Therefore, it is not suitable for long-term monitoring. Dry electrodes overcome this issue by not requiring any gel. There are three types of dry electrodes [14] capacitive electrodes, which have a high interface resistance; common-dry electrodes, which have the issue of staying in place; and invasive microneedle dry electrodes. The latter has the advantage of crossing the stratum corneum, which reduces impedance while avoiding the dermis and epidermis. Crossing the dermis and epidermis would result in a foreign body reaction due to the fact that it is the localization of nerves and vessels. There is no standard method for designing and growing microneedle arrays, as several reviews have shown. Micromolding and MRLD offer the best tradeoff in terms of quality, cost, and production efficiency.

Looking at the literature, one particular device stands out for micromolding: the Miuri-Ori structured flexible microneedle array [29]. Not only does it allow for long-term monitoring thanks to its dry microneedles, but it also resists sweat better due to its particular geometry. Its low-cost fabrication process is also particularly appealing, as well as its bending properties. We aim to achieve similar results with our device, neglecting the sweat due to our particular application. Concerning the MRLD method, the work of Ren and all [41] is of interest and has served as main inspiration for our device.

3 Our Product

3.1 Description

3.1.1 Choice of Muscles

The device can be adapted to record any muscle, provided that the reference electrode is placed on an electrically isolated muscle[1] as show on figure 1 and the length of the wires between the reference electrode and the recording electrode is adjusted, see figure 2. If the recording of several muscles is required simultaneously, multiple devices will be needed as each device can only record one muscle at a time. Proper electrode placement is crucial as it directly affects the signal integrity.

The choice of the muscle to target is driven by the size of the muscle, and its importance in major arm movement. Big muscles are favoured because the signal is easier to detect. In addition, we favour muscles of the superficial layer, that are closer to the surface. [30] In addition, triceps are particularly prone to spasm [11]. Targeted muscles will also be selected depending on the patient.

Regarding Laura, as movements are only perceived from the upper body, including the eyes, the following muscles can be targeted: triceps brachii, biceps brachii (2 major muscles of the arm), extensor carpi ulnaris (adduction as well as extension of the wrist [30] and brachioradialis (the flexor at the elbow).

For illustrative purposes, we have chosen to focus solely on the *biceps brachii*.

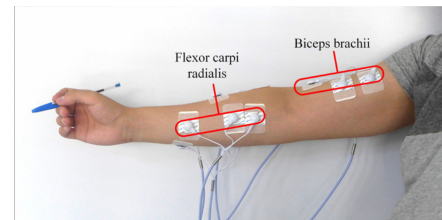


Figure 1: Example of EMG electrode placement for the main muscles of the arm and forearm [17]

3.1.2 Building blocks

The total system is composed of 5 main building blocks as shown on figure 2:

1. The transducer, made of a recording electrode placed on the target tissue (*biceps brachii* on the arm)
2. The reference electrode placed on an electrically unrelated muscle (*brachio radialis* on the elbow)
3. The electronic system (amplification and digitisation) and the battery (see section 3.4 Electronic System), connected to (1) and (2) with wires. The signal is sent to (4) wirelessly.
4. The signal processing unit, receives the system and applies an algorithm that distinguishes between voluntary movements and spasms based on a threshold measurement. It then sends a feedback (5) to the patient accordingly.
5. The feedback system, which could be vibration or light, communicates to the patient the nature of the movement.

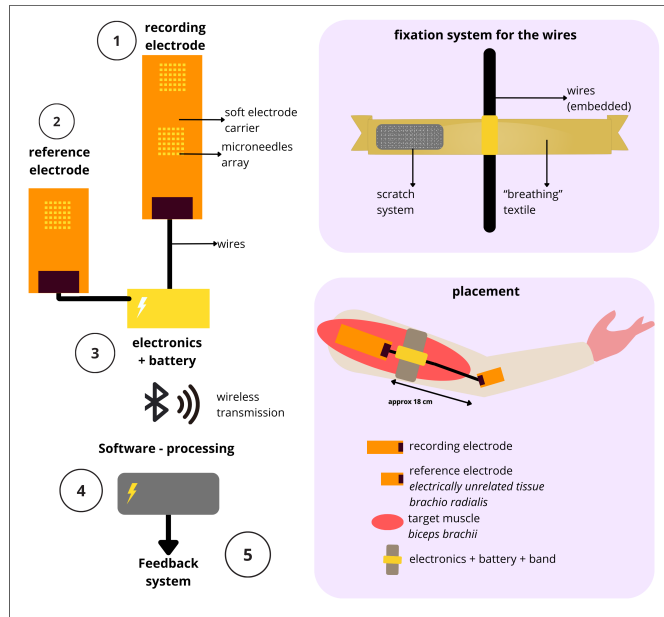


Figure 2: Building blocks of the device

Our device focuses on the measurement component; the transducer (1, 2) and the electronic system (3). Leaving the signal processing(4) and feedback(5) for further development.

As we can see in figure 2, the wires connecting the reference electrode to the electronics, the chip and the battery, are embedded in a breathable elastic textile secured with velcro ([8] around the arm to prevent the cables from getting tangled up.

3.2 Process flow

3.2.1 Dimensions

The FMAE is a square of a *6 by 6* microneedles. To penetrate the stratum Corneum (SC) layer of the skin without hurting the patient, the height of the needles is $500 \mu\text{m}$ [23]. It is a common size in the literature where it ranges from $400 \mu\text{m}$ to $600 \mu\text{m}$, as seen in [26, 41, 45, 29, 40]. The pitch between the needles is $800 \mu\text{m}$. The base and tip diameters of the needle are $300 \mu\text{m}$ and $10 \mu\text{m}$ respectively, leading to a small array area of 18.5 mm^2 . As calculated in Annex7, the total conductive area is 25 mm^2 , and a microneedles have a conductive surface on 0.25 mm^2 .

On the recording electrode, the two microneedle arrays (anode and cathode) are separated by 2.5 cm to record effectively EMG signals [27]. The recording and the

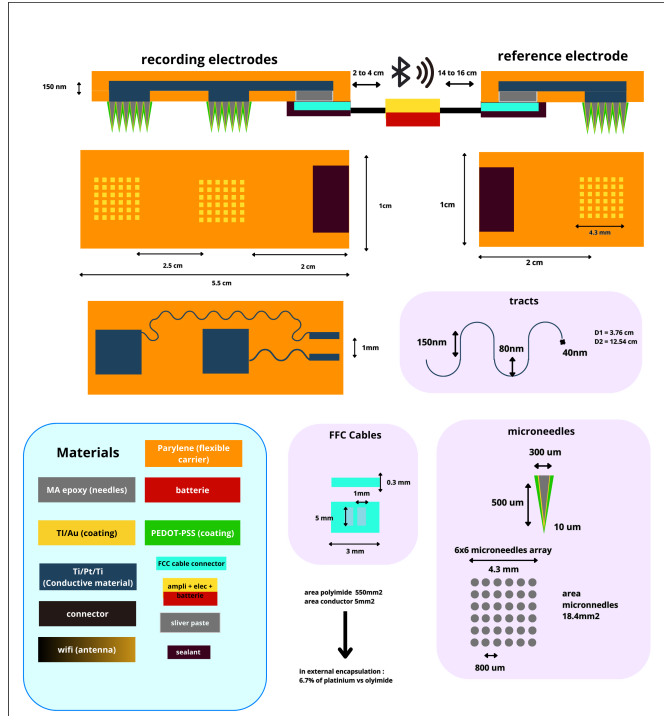


Figure 3: Full design and dimension of the device

reference electrode are separated by approximately 18 cm, which is an approximation of the distance between our target muscle and the elbow in children of Laura's age [10].

The conductive tracks follow a serpentine pattern as seen in [22] to authorise flexibility and stretchability. We dimensioned the serpentine shape according to the paper result to obtain the best flexibility while keeping good functionality.

3.2.2 Connectors

We integrated an FFC cable to our electrodes to deliver the signal while keeping flexibility. We dimensioned the electrode for a 100P3NNDLLL-510510 classic FFC from Nicomatic, with only two entries separated by a 1.00 mm pitch [2]. The FFC could be connected to the electronics or another, less flexible but more robust, cable to go to the electronics. Using a modular connector [16], could also allow to change separately the electronics and the electrode if needed.

3.2.3 Process flow steps

The most important steps of the process flow of the recording electrode are described in the text, but all the steps are presented in detail in the figures 4 and 5. The schematic of the final devices is shown at the top of figure 3.

First, a 25 μm bottom encapsulation layer of Parylene PI-2611 [36] is spin-coated on a silicon wafer disc with a sacrificial layer.. A 25 μm /150 μm /25 μm conductive layer of Ti/Pt/Ti is sputtered. The tracks are defined thanks to negative photolithography development and dry etching and follow the serpentine shape explicated before. A symmetric 25 μm top encapsulation layer of Parylene is spin-coated. We defined the thickness of the encapsulation to ensure manipulation and isolation of the device while being soft enough to follow the radius of the arm (see 3.3.2).

We then produce the electrode arrays. Two squares of the size of the microneedle array are etched in the top encapsulation layer and filled with platinum. This is done via successive steps of photolithography and dry etching shown in figure 5 while managing space for the FFC connector. Next, the microneedle arrays (MA) are drawn on the conductive layer using the additive MRDL method. MA is coated with Ti/Au and treated with PDOT::PDSS to ensure conductivity. Finally, the FFC is placed and the sacrificial layer is dissolved to release the probe.

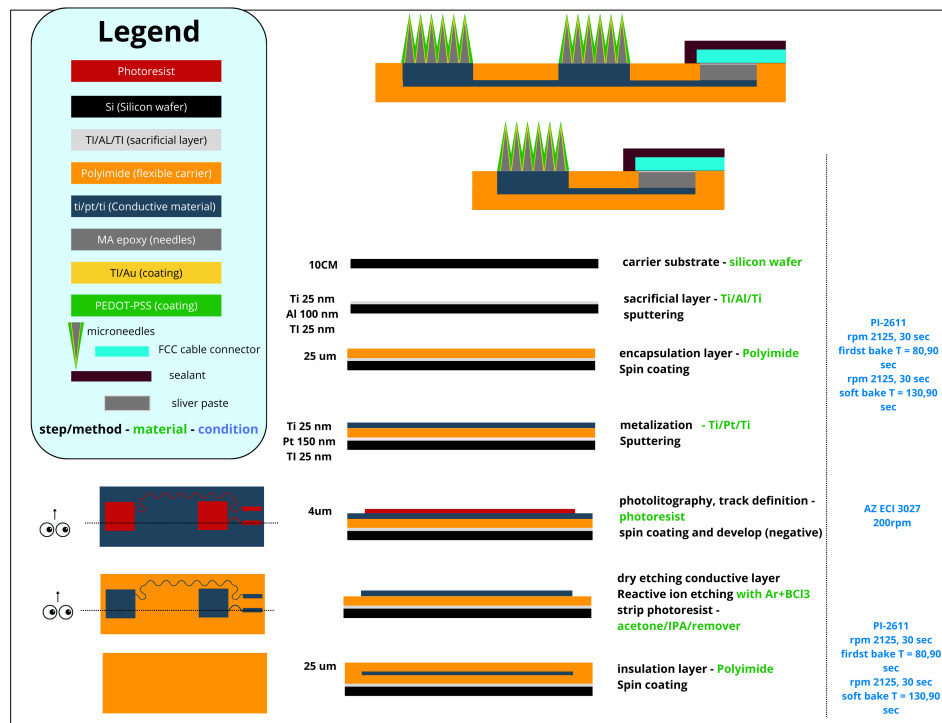


Figure 4: Process flow, part 1

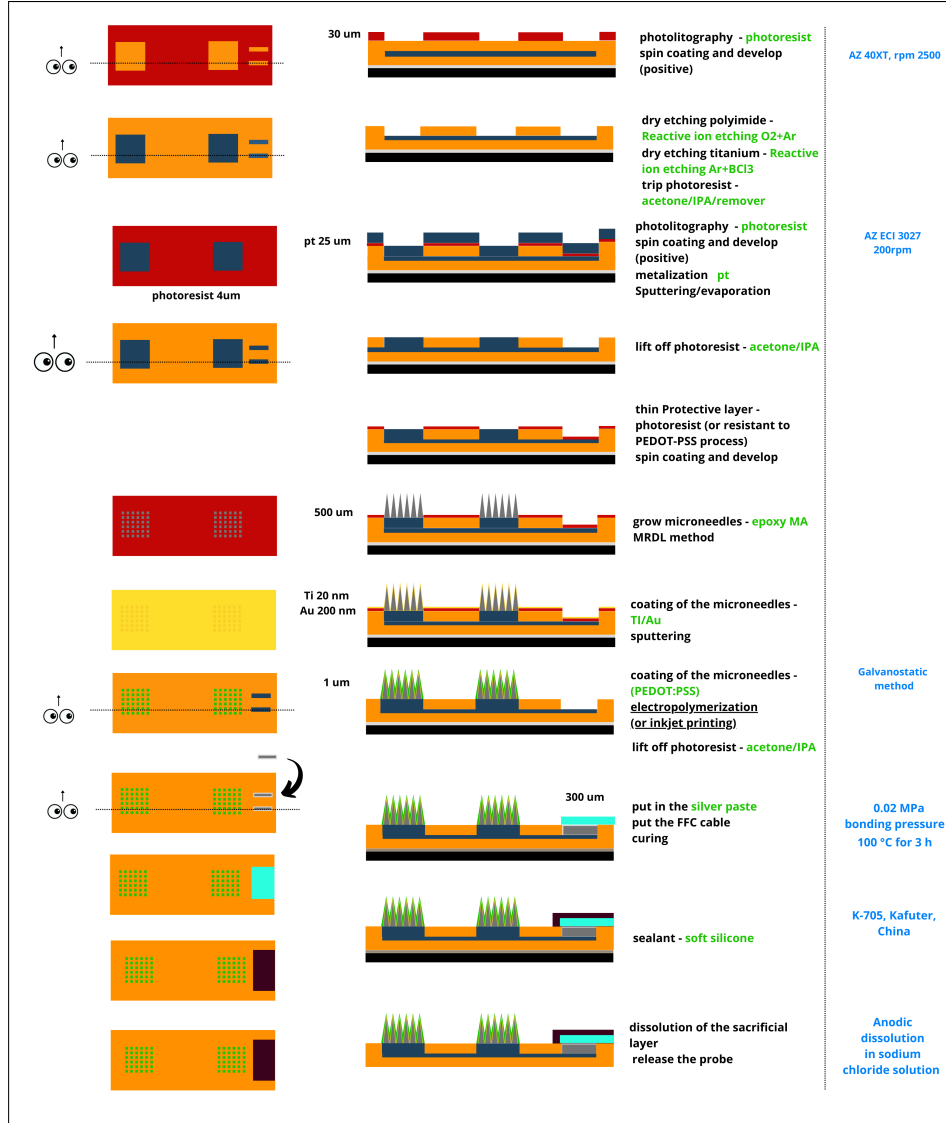


Figure 5: Process flow, part 2

Choice of MRDL method:

Our understanding of the Magnetorheological Drawing Lithography (MRDL) technique is primarily based on these two research papers: [12] and [41]. As it is explained in [41] the traditional methods employed for fabricating microneedle arrays (MA) include lithography with etching, micromolding, laser machining, 3D printing, thermal drawing, and magnetization-induced self-assembling. Typically, these arrays are produced on rigid substrates such as silicon, stainless steel, copper and polymethyl methacrylate (PMMA). However, there is limited exploration of flexible substrate fabrication due to the inherent complexity of the process. Notably, attempts have been made to introduce flexibility in MA design but the curved substrate remained rigid. Similarly, a flexible parylene-based MA aimed at long-term bio-potential monitoring but featured a highly intricate and expensive fabrication process, including thermal oxidation, reactive-ion etching, parylene film deposition, lift-off technique, and sputtering. Another effort introduced a flexible polymer photoresist-based MAE suitable for large-scale production, employing UV maskless lithography. However, this method necessitates expensive and sophisticated equipment located in clean rooms.

MRDL is a novel fabrication approach utilising a Curable Magnetorheological Fluid (CMRF) that is an oil-type carrier fluid housing $1 \mu\text{m}$ sized magnetic particles responding to a magnetic field generated by simple magnets. This magnetic response, in conjunction with gravitational forces and surface tension, enables the controlled formation and solidification of droplets into needles. Information on the feasibility of this novel technique is detailed in the Feasibility

assessment 4.1 section.

3.3 Characterisation

3.3.1 Impedance of the electrodes

The impedance of the electrodes depends on the conductivity of each coating layer of the electrode and the shape and number of needles. In this study [41] and the corresponding graph 16, the number of needles needs to be strictly superior to 18 to obtain an equivalent or better result than Ag/Cl electrodes. We have 36 needles for each array, which corresponds to an impedance in the range of $0 - 100k\Omega$ in the paper [41]. We tried to calculate an approximation of the resistance of the device [7Annex](#).

3.3.2 Stress on the device, bending stiffness

Our devices will have to conform to the radius of a child's arm as much as possible. We need to assess the stress applied to the probe on each layer to ensure that it will support the bending. All the plots and results can be found on figure 6, code in annexes [7](#)

Main materials properties have been listed in table 2 and we tested radius from 2 to 6 cm. We neglected the micro-needles and FFC region. According to this paper [2], the FFC is flexible enough.

The models have been separated into two regions. The connective region is the part of the probe composed of the two encapsulation layers and a conductive layer in the middle (between the two electrodes and between the electrodes and the FFC). In this region we placed the neutral plane in the conductive layer. At the minimal radius, the stress is negligible in every layer, with a maximum of 6MPa on the top of the encapsulation (see figure 18).

The second region is the MA region with a different structure. A platinum layer connects the conductive layer to the needles, making the probe region half platinum. In this case, the neutral plane ends up in the middle of the platinum layer. The maximum stress is at the conductive layer and at the top of the platinum layer (to the microneedles), around 100 MPa (see figure 18). This could represent a limitation for our design. The limit radius is 2 cm, but it doesn't exceed the tensile strength of the platinum and decreases rapidly with a superior radius.

The bending stiffness of the device is approximately $30, \mu Pa$.

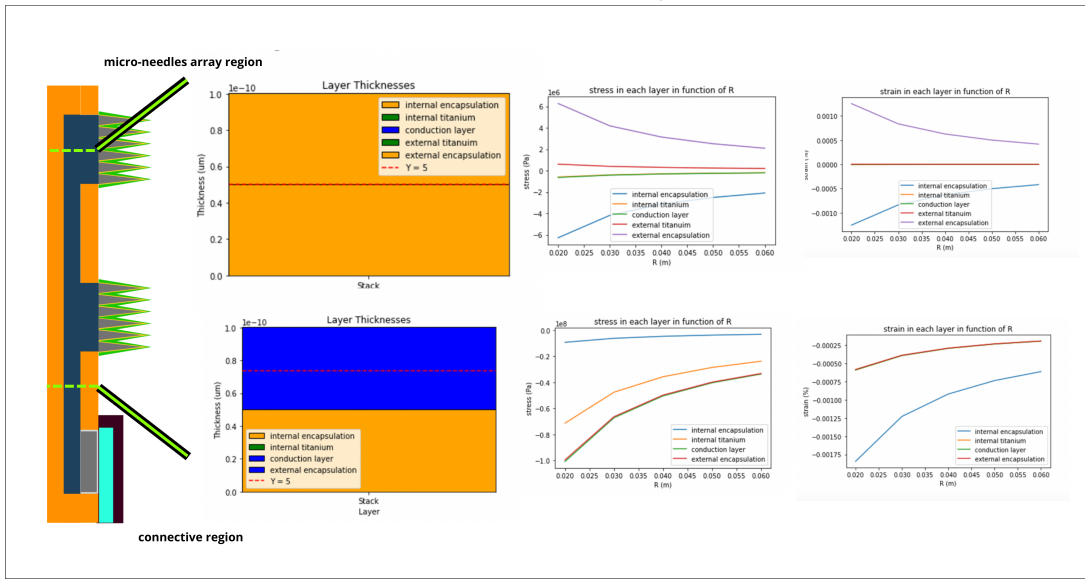


Figure 6: Plot of the neutral plane, stress and strain on each layer for radius $r \in [2, 6]cm$. The calculation are shown in figure [7](#)

3.3.3 Other characterisation steps

Other characterisation step needs to be conducted on the devices. Notably, the stiffness and the impedance, approximated before, would need to be tested empirically. Multiple additional tests should be conducted.

Some characterisation steps are specific to microneedles [41]; First, we will conduct a fracture performance assessment, measuring the stress during the insertion and the removal and the limit of our devices. We will perform an axial and transversal force mechanical test and detect failure by the decrease of a sudden decrease of force. Second, we will assess the penetration performance by simulating the insertion process with a non-linear finite element model, and will insertion test with different forces. We will finally assess the signal-to-noise ratio and the electrode-skin interface impedance (EII) during the insertion process and after.

Finally, we will have to test how long the electrodes stay viable and usable.

3.4 Electronic System

To be able to transfer the EMG data wirelessly to the signal processing unit, our device needs a built-in electronic system (see Fig. 7). It needs to filter out the noise appropriately, amplify the signals of interest, compress the processed data and then finally transmit it. To execute these actions, our system is comprised of an amplifier, an analog to digital converter (ADC), a microcontroller and a Bluetooth module, as detailed below. For its design, both the frequencies as well as the amplitudes of the signals must be taken into account, to precisely handle the data. In recorded EMG signals, these values can take place within a wide range (frequency between 0 and 10000 Hz, and amplitude between 0 and 500 mV [44]). For the design, theoretical values were taken within intervals as summarised in table 9. For the optimisation of our system, these values should be further readjusted following measurements from our developed FMAE electrodes on various patients. Each component was chosen taking into account a reasonable dimension and power consumption; as the device is not inside the body, its dimensions and power consumption do not need to be critically small. However, as the device will be worn, for reasons such as comfort, practicality and mobility, it should be as small as possible. It should also be low power as to release little heat to avoid skin irritations and burns. Other systems contain similar layouts [25, 42, 33], and were taken into account when creating our design.

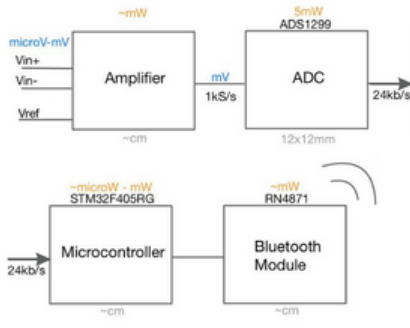


Figure 7: Electronic system for active signal acquisition, wireless transmission & approximate power consumption & dimensions

3.4.1 Amplifier

The amplifier system was designed taking the following elements into account:

Differential amplification: To measure the EMG signal, the difference between the two input electrodes is amplified. This will automatically remove any local noise that is present on both channels [4] (e.g. cardiac signals). The amplifier selected is an OTA (Operational Transconductance Amplifier) in an AC-coupled circuit (see Fig. 11). The reference electrode is used to give common ground for the differential pair. It needs to be placed on electrically neutral tissue in order to reduce or eliminate power line interference [4].

	Amplitude	Frequency
Signal: mvmnt/s-pasm	[10 μ V, 10 mV]	[20, 500] Hz
Grid noise	5 μ V/rms	50 Hz + harmonics
Movement noise	5 μ V/rms	<20 Hz
Other noise	5 μ V/rms	500 Hz <

Figure 9: Theoretical input data [3, 33] for system design

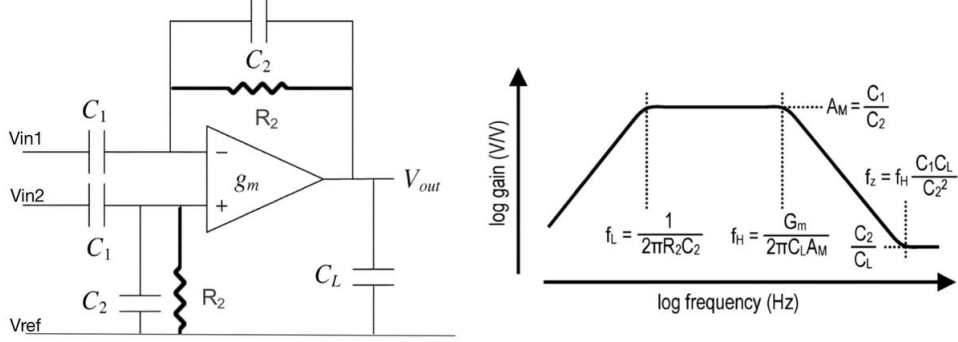


Figure 11: Capacitive feedback amplifier [19]

Input impedance: The input impedance of the circuit should be high (order of $G\Omega$) to not alter the recorded signal [5]. The input capacitances C_1 have an impedance of $Z = \frac{1}{2\pi f C_1}$. Therefore, C_1 should be as small as possible.

Programmable gain: When designing amplification circuits for EMG signals, it is crucial to ensure that the system can effectively capture and process the full amplitude range of signals that are relevant to the intended application. The dynamic range of our signals is rather large (see Tab. 9). It is largely dependent on the amount of fibres mobilised for movement and is variable across patients. For our device to be usable at different levels, we decided to implement a programmable gain: the amplifier can be tuned at different gain levels depending on the input signal, thanks to a series of switches and a comparator circuit (see Fig. 12). The different gain levels chosen were 1000, 100 and 10, to ensure a $\sim mV$ output voltage for the ADC, regardless of the signal amplitude range. This corresponds to $C_u = 1.6 \cdot 10^{-3} pF$ and $R_u = 49 G\Omega$ (for details of calculations see Fig. 19).

Filtering: The signals of interest lie between the 20 and 500 Hz range (see Tab. 9). This range is large to adapt to patients abilities. Further filtering can be done if the signals need to be narrowed down in the signal processing unit (element (4) on Fig. 2).

Number of stages:

As the amplifier is not restricted in its size, it only has one stage to ensure signal stability (for dimensions of the capacitors, see Fig. 19).

3.4.2 Analog to digital converter

The ADC was chosen taking into account the following features: (a) the sampling frequency should be 1kS/s (Nyquist rate = $2f_{max} = 1000 Hz$), (b) the minimum resolution is of 11 bits (for calculation details, see Fig. 20), (c) it needs to be in the mm range for reasons stated previously, (d) it needs to have a power consumption in the mW range.

ADS1299 [1] has these characterisations and has been used in other similar systems [25]. It

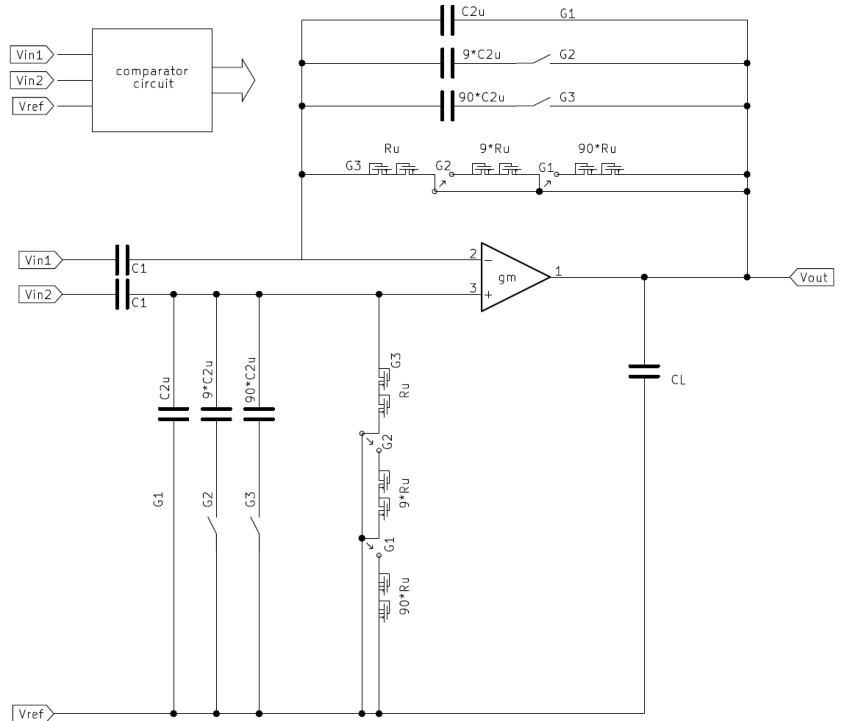


Figure 12: Amplification circuit with programmable gain tuned using a series of switches receiving inputs from a comparator circuit Schematic made with KiCad

therefore was chosen for our system.

3.4.3 Microcontroller and Bluetooth module

The microcontroller processes the data (eg. compression) for the Bluetooth transmission. The necessary characteristics for these two components are: (a) they need to be in the mm range, and (b) have a power consumption in the mW range. Many components that can be found on the market satisfy these conditions. An example of these modules are the MCU STM32F405RG [6] and the RN4871 [7].

3.4.4 Battery

The amplifier, ADC, microcontroller, and Bluetooth module all have a power supply lower than $3 V$ [6, 7]. To accommodate for this power, a $3.7V$ lithium-ion battery, for example, the ICP422339PR [3] was chosen. The battery life is then $Battery\ life\ (h) = \frac{Battery\ capacity\ (mAH)}{power\ consumption\ (mW)}$, in the worst case of let's say $50mW$ consumption, $\frac{340\ mAH}{50\ mW} = 6.8\ h$. As the device would be worn daily, in the worst case it would need to be charged 1 time during the day.

It should be noted that the mW range of power is relatively large, which is mostly due to the choice of generic ADC and Bluetooth modules. Lower-power elements can be chosen to replace these blocks.

4 Feasibility Assessment

4.1 Feasibility of MRDL method

MRDL has the advantages of thermal drawing while dispensing with the need for a mask, light irradiation, and temperature adjustments. Renowned for its simplicity, cost-effectiveness, and ability to craft intricate structures, MRDL stands as a viable solution for large-scale production. An MRDL setup needs to be self-developed to control the deposition of the droplets at a controlled speed with a camera feedback loop, as we can see in the figure 7 in the Annex. We don't aim to re-invent the process for the preparation of the CMRF fluid and the drawing of the needles, but to use the one presented in the literature [41], the details of the CMRF preparation and additional information are provided in section 7 Annex.

4.2 Time of production

In the process flow, the most time consuming step is the $25\mu m$ platinum sputtering. According to [20], for the thickness we will take approximately $5h30$ Annex7, which is feasible.

4.3 Material and cost

We choose parylene PI-2611 [36], as it is already used at EPFL [36]. We can process by sequential step as we want a thick layer [32]. For photoresist, we also used materials that are present in the available list of the CMi [35]. PEDOT-PSS is biocompatible but the technique to apply the coating may be incompatible with the current process flow and may in this case be adapted.

4.4 Electronics

The different elements of the electronic system were chosen as to keep a realistic surface area (cm range) and reasonable power consumption to ensure a low heat dissipation ($\sim mW - W$ range).

As for the production of the device, the ADC, Bluetooth module, microcontroller and battery are elements that can be bought off the shelf. The amplifier was designed following a previously used differential capacitive feedback amplifier as seen in the course (see figure 11), to stay as realistic as possible.

For this project, the programmable gain was described without going into the details of initial

calibration. Both the comparator circuit as well as the switches would need to be designed for the amplifier to be realisable (see figure 12). The amplifier could then be tested (on any CAD software). For a clean and compact device, a simple PCB could also be designed to accommodate the circuit elements. Once designed, the circuit's different elements can be bought off the shelf (capacitive and pseudo-resistance elements were checked to exist on *Mouser*), and soldered onto the board. Electronic testing should then be realised. For every step of this process, the materials and tools exist in many labs of the EPFL campus. The realisation of such a system can be estimated as taking an academic semester.

4.5 Regulation

In the European Union (EU), medical devices must undergo a conformity assessment to demonstrate compliance with legal requirements, ensuring their safety and intended performance. Regulation occurs at the EU Member State level, with the European Medicines Agency (EMA) playing a role in the regulatory process [28]. Key ISO standards play a pivotal role in upholding the quality and safety of medical devices. While certification is optional, organisations can derive substantial benefits from implementing this standard. It is applicable to entities engaged in medical device activities and assists certification bodies in their auditing processes. Our device must conform to the ISO standards listed below:

ISO 13485: This standard outlines requirements for a quality management system governing the design, development, production, installation, and servicing of medical devices. **ISO 14971:** Focused on medical device risk management, this standard is indispensable for ensuring the safety and effectiveness of devices. **ISO 10993:** Addressing the bio-compatibility of the device, which is particularly relevant in the context of paediatric patients.

5 Conclusion

Our device integrates distinct features identified individually in studies on dry electrodes for bio-signal monitoring, and introduces innovation by assembling them into a cohesive design. Particularly uncommon is the fusion of an active system, featuring pre-amplification modules near the electrode, with Flexible Microelectrode Arrays (FMAEs).

A notable aspect of our design is the utilisation of the Magnetorheological Drawing Lithography (MRDL) technique for fabricating the micro-needle array (MA). This method offers a rapid and cost-effective fabrication process, eliminating the need for a clean room. The incorporation of wireless communication, specifically Bluetooth, at the terminal stage of the data chain enhances electrode wearability.

Our system will be more convenient for children and patients with strong spasms as it contains fewer wires, requires no gels and doesn't hurt [23], and allows long-term monitoring, which wasn't the case with the previous design.

Ensuring modularity across patients, we implemented a programmable gain. Our system, with fewer wires, no gels, and painless application [23], is particularly convenient for children and patients with strong spasms, enabling long-term monitoring, a significant improvement over previous designs.

However, our device has limitations. The use of expensive techniques like lithography (for the substrate) and the necessity for clean room production restrict its scalability. Exploring alternatives, Direct Laser Writing could be employed for the conductive layers, offering cost-effectiveness [41].

Regarding the microneedle array production, while this report details the MRDL method, the micro-molding technique also presents advantages, particularly in terms of simplicity in the process flow and suitability for mass production [26].

We had several options to produce the microneedle array. In this report, we decided to present the process flow that uses the MRDL method, but the micro-molding technique also has many advantages. After reflection and reconsideration, we would rather use the micro-molding method

that seems easier to produce with fewer steps in the process flow and that is more suitable for mass production [26].

Furthermore, the current solution addresses only one muscle, potentially complicating setup for monitoring multiple muscles. Considering cable length dependence on the targeted muscle, we propose embedding additional cable length in the electronics-containing band, although this fixation method requires testing. Similarly, patches may be necessary for more efficient electrode fixation.

Lastly, although the employed techniques are well-known, our unique electrode and amplifier design necessitates additional time for production and testing, involving characterisation, safety, and calibration processes. This approach differs from using pre-existing industrial elements.

6 Appendix - Team work

The majority of the work and brainstorming has been a collaborative effort, as visible in 13.

Jennifer has been our go-to person for connecting with the therapist and has been our Swiss pocket knife, particularly diving into characterisation, microneedles and electrodes alongside Jean-Baptiste. Jean-Baptiste has also been essential in uncovering microneedle methods and perfecting the process flow with Jade. Jade also worked on characterisation, dimension and connectors, while being the canvas design manager. And let's not forget Ivonne, our electronics maestro overseeing the entire system's dimensioning.

The team had a productive dynamic and was willing to put in extra hours to achieve the present result. Each member contributed to both the presentations and the report, whether it was through reading, writing, or designing. Therefore, it is difficult to attribute individual contributions. We achieve teamwork and are proud of it! Overall, we are all incredibly grateful!



Figure 13: Team working together in front of their different work whiteboards

References

- [1] URL: <http://www.sfu.ca/~dmackey/Chap%203-4%20EMG.pdf> (visited on 27/12/2023).
- [2] URL: https://people.ece.cornell.edu/land/courses/ece5030/labs/f2009/EMG_measurement_and_recording.pdf (visited on 27/12/2023).
- [3] URL: <https://www.hilarispublisher.com/open-access/mechanical-behaviour-of-skin-a-review-2169-0022-1000254.pdf> (visited on 30/12/2023).
- [4] URL: <https://www.renata.com/en-ch/downloads/?product=icp422339pr&fileid=526a15a964fb49127a9e8d773c> (visited on 28/12/2023).
- [5] URL: <https://www.mouser.ch/datasheet/2/389/stm32f405rg-1851084.pdf> (visited on 27/12/2023).
- [6] URL: <https://www.premus2004.ethz.ch/NDSAG/Tutorial%20Delsys%20Surface%20EMG%20intro.pdf> (visited on 27/12/2023).
- [7] URL: <https://www.ti.com/lit/ds/symlink/ads1299-6.pdf?ts=1702026596123> (visited on 27/12/2023).
- [8] *7.22zl 50% OFF—1 Stuk Elastische Ademende Sport Pols Knie Enkel Elleboog Kuit Armband Brace Ondersteuning Wrap— — - AliExpress.* nl. URL: https://nl.aliexpress.com/item/1005006169351130.html?src=ibdm_d03p0558e02r02&sk=UneMJZVf&aff_platform=aaf&aff_trace_key=72c50d792b1b4c309d637f76afff2768-1703922571289-08978-UneMJZVf&af=&cv=&cn=&dp= (visited on 30/12/2023).
- [9] *A Table of Electrical Conductivity and Resistivity of Common Materials.* en. Section: ThoughtCo. URL: <https://www.thoughtco.com/table-of-electrical-resistivity-conductivity-608499> (visited on 28/12/2023).
- [10] Joshua M. Abzug et al. “Establishment of Normal Ranges of Upper Extremity Length, Circumference and Rate of Growth in the Pediatric Population”. In: *Pediatrics* 144.2_MeetingAbstract (Aug. 2019), p. 790. ISSN: 0031-4005. DOI: [10.1542/peds.144.2MA8.790](https://doi.org/10.1542/peds.144.2MA8.790). URL: <https://doi.org/10.1542/peds.144.2MA8.790> (visited on 29/12/2023).
- [11] William Bozeman. *Muscle Spasm in Tricep: Causes, Treatments, And Prevention.* en-US. Section: Muscle Spasms. May 2023. URL: <https://neuragenex.com/understanding-why-muscle-spasm-in-tricep-occurs/> (visited on 27/12/2023).
- [12] Zhipeng Chen et al. “Rapid fabrication of microneedles using magnetorheological drawing lithography”. In: *Acta Biomaterialia* 65 (Jan. 2018), pp. 283–291. ISSN: 1742-7061. DOI: [10.1016/j.actbio.2017.10.030](https://doi.org/10.1016/j.actbio.2017.10.030). URL: <https://www.sciencedirect.com/science/article/pii/S174270611730658X> (visited on 27/12/2023).
- [13] *Cyton Biosensing Board (8-channels).* en. URL: <https://shop.openbci.com/products/cyton-biosensing-board-8-channel> (visited on 28/12/2023).
- [14] *Development of soft dry electrodes: from materials to structure design.* URL: <https://www.oaepublish.com/articles/ss.2023.16> (visited on 30/12/2023).
- [15] *Elements Electrical Conductivity Reference Table – Angstrom Sciences.* URL: <https://www.angstromsciences.com/elements-electrical-conductivity> (visited on 28/12/2023).
- [16] *FI-RC3-1B-1E-15000 JAE Electronics — Mouser.* de-ch. URL: <https://www.mouser.ch/ProductDetail/656-FIRC31B1E15000> (visited on 27/12/2023).
- [17] *Figure 2: Electrode placement over the forearm and upper arm muscles.* en. URL: https://www.researchgate.net/figure/Electrode-placement-over-the-forearm-and-upper-arm-muscles_fig3_309174529 (visited on 27/12/2023).
- [18] AJ Gallagher, Aisling Ní Annaidh and Karine Bruyère-Garnier. “Dynamic tensile properties of human skin”. In: *2012 IRCOBI Conference Proc* (Jan. 2012), pp. 12–14.

- [19] R.R. Harrison and C. Charles. “A low-power low-noise CMOS amplifier for neural recording applications”. In: *Solid-State Circuits, IEEE Journal of* 38 (July 2003), pp. 958–965. DOI: [10.1109/JSSC.2003.811979](https://doi.org/10.1109/JSSC.2003.811979).
- [20] *High-Rate Sputtering of the Platinum Metals*. en-GB. URL: <https://technology.matthey.com/journal> (visited on 30/12/2023).
- [21] Ehsan Hosseini, Vinayaraj Ozhukil Kollath and Kunal Karan. “The key mechanism of conductivity in PEDOT:PSS thin films exposed by anomalous conduction behaviour upon solvent-doping and sulfuric acid post-treatment”. en. In: *Journal of Materials Chemistry C* 8.12 (Mar. 2020). Publisher: The Royal Society of Chemistry, pp. 3982–3990. ISSN: 2050-7534. DOI: [10.1039/C9TC06311K](https://doi.org/10.1039/C9TC06311K). URL: <https://pubs.rsc.org/en/content/articlelanding/2020/tc/c9tc06311k> (visited on 28/12/2023).
- [22] Bowen Ji et al. “Stretchable Parylene-C electrodes enabled by serpentine structures on arbitrary elastomers by silicone rubber adhesive”. In: *Journal of Materiomics* 6.2 (June 2020), pp. 330–338. ISSN: 2352-8478. DOI: [10.1016/j.jmat.2019.11.006](https://doi.org/10.1016/j.jmat.2019.11.006). URL: <https://www.sciencedirect.com/science/article/pii/S2352847819302230> (visited on 27/12/2023).
- [23] Peter B. Kang et al. “Utility and practice of electrodiagnostic testing in the pediatric population: An AANEM consensus statement”. eng. In: *Muscle & Nerve* 61.2 (Feb. 2020), pp. 143–155. ISSN: 1097-4598. DOI: [10.1002/mus.26752](https://doi.org/10.1002/mus.26752).
- [24] *Kendall EMG/ECG Foam Solid Gel Electrodes*. en. URL: <https://shop.openbci.com/products/kendall-emg-ecg-foam-solid-gel-electrodes-30-pack> (visited on 28/12/2023).
- [25] Kunwoo Lee et al. “Wireless Epidermal Electromyogram Sensing System”. In: *Electronics* 9 (Feb. 2020), p. 269. DOI: [10.3390/electronics9020269](https://doi.org/10.3390/electronics9020269).
- [26] Junshi Li et al. “High-Performance Flexible Microneedle Array as a Low-Impedance Surface Biopotential Dry Electrode for Wearable Electrophysiological Recording and Polyso-mnography”. en. In: *Nano-Micro Letters* 14.1 (June 2022), p. 132. ISSN: 2150-5551. DOI: [10.1007/s40820-022-00870-0](https://doi.org/10.1007/s40820-022-00870-0). URL: <https://doi.org/10.1007/s40820-022-00870-0> (visited on 28/12/2023).
- [27] Jiaao Lu et al. “High-performance Flexible Microelectrode Array with PEDOT:PSS Coated 3D Micro-cones for Electromyographic Recording”. In: *2022 44th Annual International Conference of the IEEE Engineering in Medicine & Biology Society (EMBC)*. ISSN: 2694-0604. July 2022, pp. 5111–5114. DOI: [10.1109/EMBC48229.2022.9871052](https://doi.org/10.1109/EMBC48229.2022.9871052). URL: <https://ieeexplore.ieee.org/document/9871052> (visited on 29/12/2023).
- [28] *Medical devices — European Medicines Agency*. URL: <https://www.ema.europa.eu/en/human-regulatory-overview/medical-devices#ema-inpage-item-13035> (visited on 30/12/2023).
- [29] *Miura-ori structured flexible microneedle array electrode for biosignal recording — Microsystems & Nanoengineering*. URL: <https://www.nature.com/articles/s41378-021-00259-w> (visited on 27/12/2023).
- [30] *Muscles of the Posterior Forearm - Superficial - Deep - TeachMeAnatomy*. URL: <https://teachmeanatomy.info/upper-limb/muscles/posterior-forearm/> (visited on 28/12/2023).
- [31] Xin Niu et al. “Surface bioelectric dry Electrodes: A review”. In: *Measurement* 183 (Oct. 2021), p. 109774. ISSN: 0263-2241. DOI: [10.1016/j.measurement.2021.109774](https://doi.org/10.1016/j.measurement.2021.109774). URL: <https://www.sciencedirect.com/science/article/pii/S0263224121007296> (visited on 30/12/2023).
- [32] *Parameters to make Polyimide Film (PI-2600) with Thickness more than 100 um*. en. URL: https://www.researchgate.net/post/Parameters_to_make_Polyimide_Film_PI-2600_with_Thickness_more_than_100_um (visited on 30/12/2023).

- [33] Akbar Pashaei, Mohammad Reza Yazdchi and Hamid Reza Marateb. "Designing a Low-noise, High-resolution, and Portable Four Channel Acquisition System for Recording Surface Electromyographic Signal". In: *Journal of Medical Signals and Sensors* 5.4 (2015), pp. 245–252. ISSN: 2228-7477. URL: <https://www.ncbi.nlm.nih.gov/pmc/articles/PMC4759841/> (visited on 27/12/2023).
- [34] Dilip R. Patel et al. "Cerebral palsy in children: a clinical overview". en. In: *Translational Pediatrics* 9.Suppl 1 (Feb. 2020). Publisher: AME Publications, S125. DOI: [10.21037/tp.2020.01.01](https://doi.org/10.21037/tp.2020.01.01). URL: <https://www.ncbi.nlm.nih.gov/pmc/articles/PMC7082248/> (visited on 28/12/2023).
- [35] *Photoresists available in CMi.* en-GB. URL: <https://www.epfl.ch/research/facilities/cmi/process/photolithography/photoresist-selection/> (visited on 30/12/2023).
- [36] *PI 2610 & PI 2611.* en-GB. URL: <https://www.epfl.ch/research/facilities/cmi/process/photolithography/photoresist-selection/pi-2610-pi-2611/> (visited on 30/12/2023).
- [37] *Platinum (Pt) - Properties, Applications.* en. Section: Materials Article. June 2013. URL: https://www_azom_com/article.aspx?ArticleID=9235 (visited on 27/12/2023).
- [38] *Polyimide.* URL: <https://www.mit.edu/~6.777/matprops/polyimide.htm> (visited on 27/12/2023).
- [39] *Polyimide: Properties, Processing, and Applications - Matmatch.* URL: <https://matmatch.com/learn/material/polyimide> (visited on 27/12/2023).
- [40] Lei Ren et al. "Fabrication of Flexible Microneedle Array Electrodes for Wearable Bio-Signal Recording". en. In: *Sensors* 18.4 (Apr. 2018). Number: 4 Publisher: Multidisciplinary Digital Publishing Institute, p. 1191. ISSN: 1424-8220. DOI: [10.3390/s18041191](https://doi.org/10.3390/s18041191). URL: <https://www.mdpi.com/1424-8220/18/4/1191> (visited on 27/12/2023).
- [41] Lei Ren et al. "Flexible microneedle array electrode using magnetorheological drawing lithography for bio-signal monitoring". In: *Sensors and Actuators A: Physical* 268 (Dec. 2017), pp. 38–45. ISSN: 0924-4247. DOI: [10.1016/j.sna.2017.10.042](https://doi.org/10.1016/j.sna.2017.10.042). URL: <https://www.sciencedirect.com/science/article/pii/S0924424717307306> (visited on 27/12/2023).
- [42] Afraiz Tariq Satti et al. "Microneedle Array Electrode-Based Wearable EMG System for Detection of Driver Drowsiness through Steering Wheel Grip". en. In: *Sensors* 21.15 (Jan. 2021). Number: 15 Publisher: Multidisciplinary Digital Publishing Institute, p. 5091. ISSN: 1424-8220. DOI: [10.3390/s21155091](https://doi.org/10.3390/s21155091). URL: <https://www.mdpi.com/1424-8220/21/15/5091> (visited on 27/12/2023).
- [43] *Titanium Properties.* en. URL: <https://kyocera-sgstool.co.uk/titanium-resources/titanium-information-everything-you-need-to-know/titanium-properties/> (visited on 27/12/2023).
- [44] Cristian Vidal Silva, Andrew Philominraj and Carolina Río. "A DSP Practical Application: Working on ECG Signal". In: Nov. 2011. ISBN: 978-953-307-406-1. DOI: [10.5772/25499](https://doi.org/10.5772/25499).
- [45] Zhongyan Wang et al. "Multi-Channel Flexible Microneedle Electrode Array(MNEA) for High-Density Surface EMG Recording". In: *2022 IEEE 35th International Conference on Micro Electro Mechanical Systems Conference (MEMS)*. ISSN: 2160-1968. Jan. 2022, pp. 345–348. DOI: [10.1109/MEMS51670.2022.9699517](https://doi.org/10.1109/MEMS51670.2022.9699517). URL: <https://ieeexplore.ieee.org/document/9699517> (visited on 27/12/2023).

7 Annex

Dimension

The surface of a microneedle: $A = \pi a \sqrt{a^2 + h^2}$,

where $a = 150\mu\text{m}$ and $h = 500\mu\text{m}$,

$$A = 0.25 \text{ mm}^2,$$

The total surface of contact:

We have 36 microneedles $A_{\text{needles}} = 36 \cdot A = 9 \text{ mm}^2$,

Flat region between needles $A_{\text{flat}} = A_{\text{area}} - A_{\text{disc}}$,

where $A_{\text{flat}} = d^2 - 36\pi a^2$,

$$A_{\text{flat}} = 18.49 - 2.54 = 15.95 \text{ mm}^2,$$

Therefore, total surface: $A = A_{\text{needles}} + A_{\text{flat}} \approx 25 \text{ mm}^2$.

Sputtering

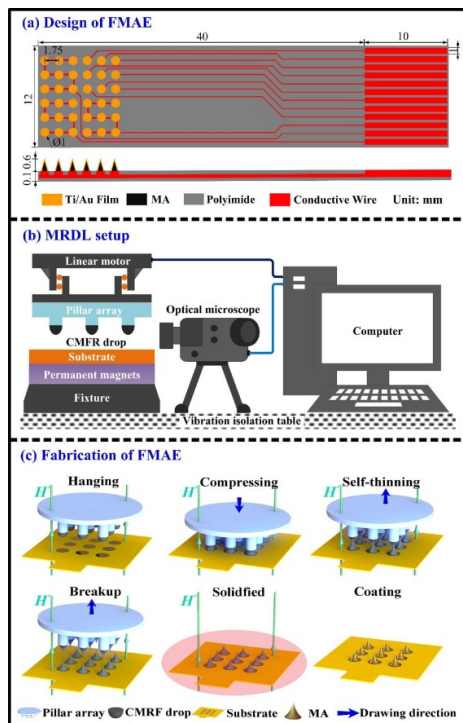
Speed sputtering: $V = 750 \times 10^{-10} \text{ m/min}$

Max thickness: $t = 25\mu\text{m}$

elapsed time: $T = t/V \approx 5h30$

MRDL method

The following information is directly extracted from the study [41].



- Firstly, the pillar tips were firstly coated with the droplets as the pillar tips were dipped in a pool of curable magnetorheological fluid (CMRF). The diameter of the copper pillar is 0.7 mm.
- Secondly, the pillars were moved toward the substrate at a speed of 1.5 mm/s by a linear motor (C-884, PI, German). The droplets were compressed on the substrate for 1 s.
- Subsequently, the pillar array was drawn back at a speed of 1.5 mm/s and stopped at a distance of 12 mm away from the substrate. A liquid MA was formed on the substrate under an external magnetic field intensity of 100 mT. The fabrication process was carried out at room temperature.
- The liquid MA was pre-baked by hot air blowing at a temperature of 95 °C for 5 min. The fabrication process was monitored by an optical microscope. The pre-baked microneedle was further solidified in a vacuum oven at a temperature of 100 °C for 1 h.
- 20 nm Ti film and 200 nm Au film were uniformly coated on the surface of solidified MA by the magnetron sputtering machine (MSP-3300, Jinsheng-weina Technology Co., Ltd, China) in sequence

CMRF preparation:

The following information is directly extracted from the study [41]. Epoxy novolac resin (Weiyi Metallography Experiment Instrument Co., LTD, China) and iron particles with an average diameter of 1 μm (Naiou Nano Technology Co., Ltd, China) were purchased. CMRF was prepared as: firstly, epoxy novolac resin was uniformly mixed with iron particles with a mass ratio of 1: 0.5. Subsequently, the mixture was pre-polymerized at 80 °C for 3 min.

Characterisation

impedance

material	Properties	
	conductivity [S/m]	sources
Gold	$4.52 * 10^7$	[15, 9]
Titanium	$2.34 * 10^6$	
PEDOT-PSS	$0.5 * 10^2 - 3.2 * 10^5$	[21]

Figure 14: Conductivity of coating materials of the needles

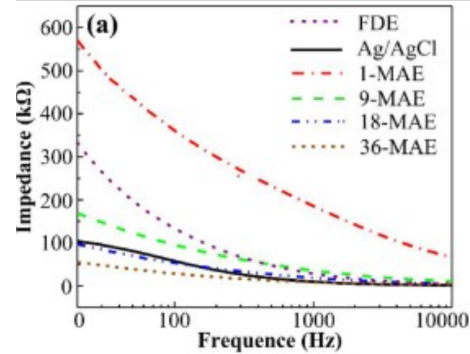
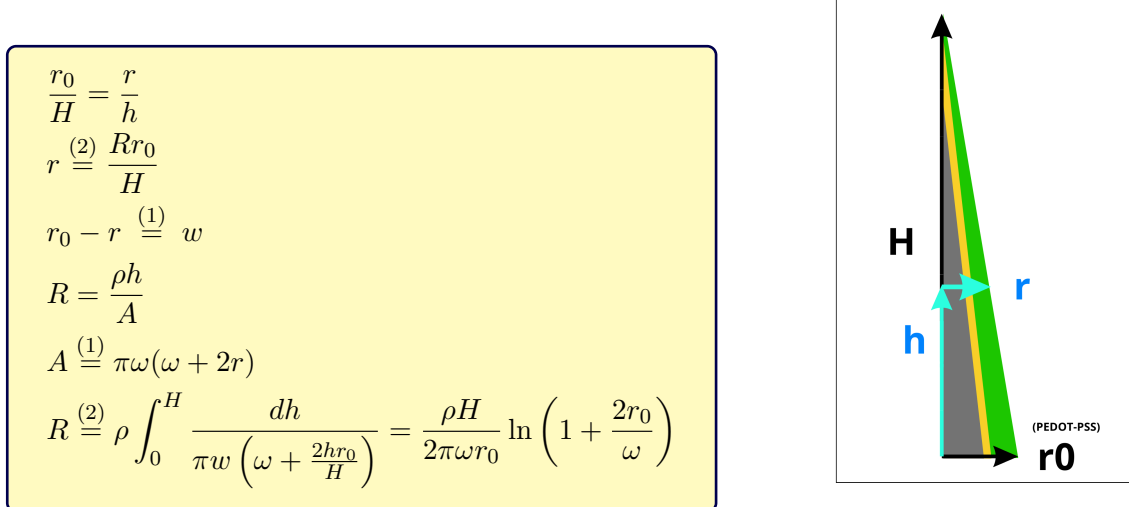


Figure 16: Impedance as a function of the frequency for different numbers of microneedles in the study [41]

r_0 is the initial radius of the layer considered, w is the width of the layer, ρ changes according to the electric material, and A is the cross-sectional area corresponding to $\pi(r_0^2 - r^2)$ and R is the resistance.



Stress, strain, bending stiffness

material	Properties		
	Elastic modulus (GPa)	tensile strength (Mpa)	sources
polyimide	1-5	110-230	[38, 39]
titanium	120	240	[43]
platinum	170	125-165	[37]
skin	$5 * 10^{-6} - 140 * 10^{-3}$	17-26	[3, 18]

Table 2: Properties of the main materials of the probe, and the skin

```

here we have E*D
for polyimide : 125000.0
for platinum film : 25500.0
ration encaps/conduct : 4.9
conduction layer [ 2.50e-05 , 2.52e-05 ]
the total tickness is 5.02e-05
the neutral plane is 2.51e-05
Bending stiffness of this part 7.25e-06 N.m2

here we have E*D
for polyimide : 125000.0
for platinum film : 25500.0
ration encaps/conduct : 4.9
conduction layer [ 2.50e-05 , 2.52e-05 ]
the total tickness is 5.02e-05
the neutral plane is 3.69e-05
Bending stiffness of this part 2.35e-05 N.m2

```

```

for internal encapsulation max stress -6 MPa
for internal titanium max stress -1 MPa
neutral plane in the conduction layer
for conduction layer max stress -1 MPa
for external titanum max stress 1 MPa
for external encapsulation max stress 6 MPa

```

```

for internal encapsulation max stress -9 MPa
for internal titanium max stress -71 MPa
for conduction layer max stress -101 MPa
neutral plane in the external encapsulation
for external encapsulation max stress -99 MPa

```

Approximate bending stiffness 3.08e-05 N.m2

Figure 18: result of the calculation of the neutral plane, stress and strain on each layer for a range of radius. The calculation are based on the course material

Electronics

We have: $\frac{C_1}{C_2} = G$, $f_l = 20Hz$, $f_h = 500Hz$, input impedance $Z_1 = 1G\Omega$

1. $Z_1 = \frac{1}{2\pi f C_1}$ let's take $f = 100Hz$ (high signal density at this frequency) $\rightarrow C_1 \approx 1.6pF$ (mm range in size)

2. For a programmable gain, C_2 will be replaced by a series of capacitors in parallel in a switch circuit to tune the gain depending on the amplitude of the input voltage. We need the smallest μV signals to be amplified by 1000, and the highest signals in the mV range should not surpass the $\sim mV$ input voltage from the ADC (see datasheet), and therefore will only be amplified by 10. An extra gain setting for intermediate signals is also implemented.

$$G_1 = 1000 \rightarrow C_{21} = C_2 u = 1.6 * 10^{-3} pF \text{ (mm range in size)}$$

$$G_2 = 100 \rightarrow C_{22} = 10C_2 u$$

$$G_3 = 10 \rightarrow C_{23} = 100C_2 u$$

3. As $R_2 = \frac{1}{2\pi f_l C_2}$, different values are created by placing resistors in series with switches:

$$G_1 = 1000 \rightarrow R_{21} = \frac{1}{2\pi f_l C_{21}} = 100R_u$$

$$G_2 = 100 \rightarrow R_{22} = \frac{1}{2\pi f_l * 10 * C_{22}} = 10R_u$$

$$G_3 = 10 \rightarrow R_{23} = R_u = \frac{1}{2\pi f_l * 100 * C_{23}} = 49G\Omega$$

Due to the size of the resistances, pseudo-resistances are used (mm range in size).

Figure 19: Differential capacitive feedback with programmable gain amplifier calculations

$$ENOB = \frac{SNDR(dB) - 1.76}{6.02}$$

$$SNDR = \frac{A_{max}}{A_{min}} = \frac{10mV}{5\mu V} = 2000$$

$$SNDB(dB) \approx 66 \text{ and } ENOB \approx 10.67$$

We can round up to 11 bits, the minimum resolution necessary.

Figure 20: ENOB calculations for minimal signal resolution

Code python

```

1  #!/usr/bin/env python3
2  # -*- coding: utf-8 -*-
3  """
4  Created on Thu Dec  7 13:09:43 2023
5
6  @author: djay
7  """
8  import matplotlib.pyplot as plt
9  import matplotlib.patches as patches
10 from matplotlib.colors import ListedColormap
11
12
13 # We assume here that the influence of the FFC and of
14 # the needles are negligeable
15
16 #data
17 Epolyimide = 5*pow(10,9); # 1-5 GPa
18 Etitanium = 120*pow(10,9);
19 EAluminium = 65*pow(10,9);
20 Eplatinum = 170*pow(10,9);
21 Eparylene = 2.5*pow(10,9); # 2-3 GPa
22 Egold = 80*pow(10,9);
23 #https://www.sciencedirect.com/science/
24 #article/pii/S1359836818323199#:~:
25 #text=Young's%20modulus%20and%20ulti
26 #mate%20tensile,n%20%3D%207)%2C%20respectively.
27 Eepoxy = 5*pow(10,9); #3-6 GPa
28
29 EFFC = 0 #ignore it
30
31 # Define a colormap for materials
32 colors = {
33     Epolyimide: 'orange',
34     Etitanium: 'green',
35     Eplatinum: 'blue',
36     EFFC: "purple",
37     Epolyimide*0.933+ Eplatinum*0.067 : "pink"
38 }
39
40 # construct our electrode
41 probe = []
42
43 ds = 25*pow(10,-6)
44 df = 150*pow(10,-9)
45 probe.append([Epolyimide,ds,"internal encapsulation"])
46 probe.append([Etitanium,25*pow(10,-9),"internal titanium"])
47 probe.append([Eplatinum,df,"conduction layer"])
48 probe.append([Etitanium,25*pow(10,-9),"external titanium"])
49 probe.append([Epolyimide,ds,"external encapsulation"])
50 #probe.append([EFFC,0.3*pow(10,-3),"FFC"])
51
52 #probe.pop() #FFC not in the following computations
53
54 # construct our electrode
55 probe_array = []
56
57 ds = 25*pow(10,-6)
58 ds2 = 25*pow(10,-6)
59 df = 150*pow(10,-9)
60 probe_array.append([Epolyimide,ds,"internal encapsulation"])
61 probe_array.append([Etitanium,25*pow(10,-9),"internal
    ↪ titanium"])
62 probe_array.append([Eplatinum,df,"conduction layer"])
63 probe_array.append([Eplatinum,ds2,"external encapsulation"])
64 #probe.append([EFFC,0.3*pow(10,-3),"FFC"])
65
66 #probe.pop() #FFC not in the following computations
67
68 def computation(probe, W) :
69     neutral = 0
70     current = 0
71     div = 0
72     thickness = 0
73
74     print("here we have E*D ")
75     print("for polyimide : ",round(Epolyimide*ds,2))
76     print("for platinum film : ",round(Eplatinum*df,2))
77     print("ration encaps/conduct :
    ↪ ",round(Epolyimide*ds/(Eplatinum*df),2))
78
79     # find neutral plane
80     for layer in probe :
81         current = thickness + layer[1]/2
82         thickness += layer[1]
83
84         if layer[2] == "conduction layer":
85             print(layer[2], "[",
    ↪ '{:.2e}'.format(thickness-layer[1]), ",",
    ↪ '{:.2e}'.format(thickness), "]")
86
87         neutral += layer[0]*layer[1]*current
88         div += layer[0]*layer[1]
89         neutral = neutral / div
90
91     print("the total thickness is", '{:.2e}'.format(thickness))
92     print("the neutral plane is", '{:.2e}'.format(neutral))
93
94
95     # calculate bending stiffness, we have a rectangular
    ↪ probe.
96     # I = Wt^3/12
97     # we will approximate
98     D = sum(W*p[0]*pow(p[1],3) for p in probe)
99
100    print("Bending stiffness of this part",
    ↪ '{:.2e}'.format(D), "N.m2")
101
102    # Extract material, thickness, and description from probe
103    materials = [layer[0] for layer in probe]
104    thicknesses = [layer[1]*pow(10,-6) for layer in probe]
105    descriptions = [layer[2] for layer in probe]
106
107    # Plotting
108    fig, ax = plt.subplots()
109
110    bottom = 0
111    for material, thickness, description in zip(materials,
    ↪ thicknesses, descriptions):
112        rect = patches.Rectangle((0, bottom), 1, thickness,
    ↪ linewidth=1, edgecolor='black',
    ↪ facecolor=colors[material], label=description)
113        ax.add_patch(rect)
114        bottom += thickness
115
116    # Add a horizontal line at y=5
117    ax.axhline(y=neutral*pow(10,-6), color='red',
    ↪ linestyle='--', label='Y = 5')
118
119    # Set axis labels and title
120    ax.set_xlabel('Layer')
121    ax.set_ylabel('Thickness (um)')
122    ax.set_title('Layer Thicknesses')
123
124    ax.set_ylim(0, sum(thicknesses))
125
126    # Set x-axis ticks and labels
127    ax.set_xticks([0.5])
128    ax.set_xticklabels(['Stack'], rotation=0, ha='center')
129
130    # Display the legend
131    ax.legend()
132
133    # Show the plot
134    plt.show()
135
136
137
138
139    R = [i * 0.01 for i in range(2, 7)]
140
141    current = 0
142    find_neutral = True
143    strain = []
144    stress = []
145
146    print("\n")
147    #find the layer of the neutral plane
148    # find strain, stress in each layer in fonction of the
    ↪ radius of curvature
149    for layer in probe :
150        if current < neutral:
151            curve_s = []
152            curve_ss = []
153            for radius in R :
154                s = (current - neutral)/radius
155                ss = layer[0]*s
156                curve_s.append(s)
157                curve_ss.append(ss)
158            strain.append(curve_s)
159            stress.append(curve_ss)
160            current += layer[1]
161        else :
162            current += layer[1]
163            curve_s = []
164            curve_ss = []
165            for radius in R :
166                s = (current - neutral)/radius
167                ss = layer[0]*s
168                curve_s.append(s)
169                curve_ss.append(ss)
170            strain.append(curve_s)
171            stress.append(curve_ss)
172
173        if neutral < current and find_neutral:
174            print("neutral plane in the",layer[2])
175            find_neutral = False
176
177        print("for",layer[2],"max stress",
    ↪ round(max(stress[-1], key=abs)*pow(10,-6)), "MPa")
178
179    print("\n")
180
181    for i in range(len(probe)):
182        plt.plot(R,strain[i],label = probe[i][2])
183
184    plt.xlabel('R (m)')

```

```

185     plt.ylabel('strain (%)')
186
187     plt.title('strain in each layer in function of R')
188     plt.legend()
189     plt.show()
190
191     # plt.plot(R,strain[-1],label = probe[-1][2])
192     # plt.title('strain in external layer in function of R')
193     # plt.legend()
194     # plt.show()
195
196     for i in range(len(probe)):
197         plt.plot(R,stress[i],label = probe[i][2])
198
199     plt.xlabel('R (m)')
200     plt.ylabel('stress (Pa)')
201     plt.title('stress in each layer in function of R')
202     plt.legend()
203     plt.show()
204
205     # plt.plot(R,stress[-1],label = probe[-1][2])
206     # plt.title('stress in external layer in function of R')
207     # plt.legend()
208     # plt.show()
209
210     for i in range(len(probe)):
211         plt.plot(strain[i],stress[i],label = probe[i][2])
212
213     plt.xlabel('strain (%)')
214     plt.ylabel('stress (Pa)')
215     plt.title('stress in each layer in function of R')
216     plt.legend()
217     plt.show()
218
219     # plt.plot(strain[-1],stress[i],label = probe[-1][2])
220     # plt.title('strain/stress in external layer in function
221     # of R')
222     # plt.legend()
223     # plt.show()
224
225
226     # we have two electrodes array of 4.3mm, we can approximate
227     # 4.64 cm of connective region (we take the end of the probe
228     # with no
229     # conductive layer and negligate the FFC)
230     # 0.86 cm of array region
231     D1 = computation(probe, 4.64*pow(10,-2))
232
233     D2 = computation(probe_array, 0.86*pow(10,-2))
234
235     D = D1+D2
236     print("Approximate bending stiffness",
237           '{:.2e}'.format(D),"N.m2")

```